Variation of Cone Photoreceptor Packing Density with Retinal Eccentricity and Age

Hongxin Song, Toco Yuen Ping Chui, Zhangyi Zhong, Ann E. Elsner, and Stephen A. Burns

PURPOSE. To study the variation of cone photoreceptor packing density across the retina in healthy subjects of different ages.

METHODS. High-resolution adaptive optics scanning laser ophthalmoscope (AOSLO) systems were used to systematically image the retinas of two groups of subjects of different ages. Ten younger subjects (age range, 22–35 years) and 10 older subjects (age range, 50–65 years) were tested. Strips of cone photoreceptors, approximately $12° \times 1.8°$ long were imaged for each of the four primary retinal meridians: superior, inferior, nasal, and temporal. Cone photoreceptors within the strips were counted, and cone photoreceptor packing density was calculated. Statistical analysis (three-way ANOVA) was used to calculate the interaction for cone photoreceptor packing density between age, meridian, and eccentricity.

RESULTS. As expected, cone photoreceptor packing density was higher close to the fovea and decreased with increasing retinal eccentricity from 0.18 to 3.5 mm (~0.6–12°). Older subjects had approximately 75% of the cone density at 0.18 mm (~0.6°), and this difference decreased rapidly with eccentricity, with the two groups having similar cone photoreceptor packing densities beyond 0.5 mm retinal eccentricity on average.

CONCLUSIONS. Cone packing density in the living human retina decreases as a function of age within the foveal center with the largest difference being found at our most central measurement site. At all ages, the retina showed meridional difference in cone densities, with cone photoreceptor packing density decreasing faster with increasing eccentricity in the vertical dimensions than in the horizontal dimensions. (*Invest Ophthalmol Vis Sci.* 2011;52:7376–7384) DOI:10.1167/iovs.11-7199

As the first stage of vision, the photoreceptors provide the spatial information to higher stages of visual processing. Packing density and arrangement of photoreceptors are related to the development, function, and evolution of the visual system.[1-4] The human cone photoreceptors distribution has the following features[2,5,6]: (1) a high peak cone packing density at the foveal center; (2) a rapid decrease in packing density within the central 2 mm of retina and then a more gradual decrease farther away; and (3) isodensity contours of cone photoreceptor distribution that are elongated along the horizontal axis, sometimes referred to as a cone streak.[2] Previous studies of the effect of aging on the retina suggest that normal aging is accompanied by photoreceptor changes. Both rod[7] and cone[8] outer segments have been reported to become disorganized with aging, especially when they are close to the fovea. Cone photopigment is also reduced with age[4,9] and Swanson et al.[10] reported that the decreased photopigment is largest in the central 1° of the retina, suggesting a change in foveal architecture with age, which is supported by findings of changes in both photopigment and macular pigment distributions.[11] However, the question of whether there is loss of cone photoreceptors with aging in the human retina is still controversial. Pandajonas et al.[12] found a loss of 37% of rods and 18% of cones extrapolated to a lifespan of 100 years. Gao et al.[13] and Curcio et al.[14] found that loss of rods occurs with age but did not find a decrease in cone density, although variability among individuals was high.[2] A limitation of these histologic approaches is that these measurements have been possible only ex vivo, which requires experimental manipulation of tissue before the measurements. The best data can only be collected in very fresh tissue, which is hard to obtain, and thus the total sample of data is relatively small and the age distribution sampling is variable.

In recent years, adaptive optics has enabled high-resolution retinal imaging, sufficient for measuring the cone packing density in vivo.[5,6,15-20] In the present study, we used state-of-the-art adaptive optics scanning laser ophthalmoscopes (AOSLO),[21,22] to measure the variation in cone photoreceptors in two normal populations that differed in age. We used the rapid acquisition capability to systematically collect data along four retinal meridians from near the fovea to approximately 12° retinal eccentricity. The cone packing density was compared as a function of retinal eccentricity, meridian, and age.

METHODS

Subjects

We tested 20 healthy subjects (22–65 years, mean 40.9 years; SD 16.0; 9 men and 11 women). All subjects received a complete eye examination, and all had best corrected visual acuity of 20/20 or better. Only the right eye of each subject was included in the study, although the instruments are routinely used for either eye. Spherical equivalent refractive errors ranged from +2.0 to −3.5 D (mean −0.73 D; SD 1.2). To convert packing density measurements to metric coordinates (in millimeters) from angular coordinates, axial length[6] was measured with a biometer (IOL Master; Carl Zeiss Meditec, Dublin, CA). For the present study, subjects with unusual axial lengths for their refractive status were not included, and the axial lengths for the 20 subjects ranged from 22.1 to 26.3 mm (mean 23.8 mm; SD 1.02).

Subjects were classified into two groups based on age. Subjects in group 1 ($n = 10$) were from 22 to 35 years old, their refractive error was from −3 to +0.5 D (mean −0.78 D; SD 0.79), and their axial length was from 22.1 to 26.1 mm (mean 23.7 mm; SD 1.09). Subjects in group 2 were from 50 to 65 years old with refractive error from

Corresponding author: Stephen A. Burns, School of Optometry, Indiana University, Bloomington, IN 47405; staburns@indiana.edu.

−3.5 to +1.5 D (mean −0.83 D; SD 1.6), and axial length was from 22.7 to 26.3 mm (mean 23.9 mm; SD 0.99). There was no statistically significant difference between groups in either axial length ($P = 0.282$) or refractive error ($P = 0.11$), respectively. Consent forms were obtained after a full explanation of the procedures and consequences of this study. Exclusion criteria for this study included any retinal or systemic disease. Some of the data (two of the younger subjects) had been included in previous studies.[5,6] The study protocol was approved by Indiana University Institutional Review Board and complied with the requirements of the Declaration of Helsinki.

Apparatus

Cone photoreceptor images were acquired with two AOSLO systems. The first is a single deformable-mirror system, which has been described in detail elsewhere.[22] During the course of the study a second AOSLO was completed, which had several practical advantages that allowed more rapid data collection. Thus, the study was finished with the second system. The two AOSLO systems were configured to produce identical sampling (1 μm/pixel for a model eye). Control experiments, the most relevant of which are described below, were performed to determine that both instruments produced comparable results in quantifying cone photoreceptor packing density.

Both systems included three integrated subsystems, with the pupil plane of each subsystem aligned to the two others and with different illumination wavelengths to allow independent manipulation and sampling to optimize the function of each subsystem. The key component was an SLO-based, high-magnification retinal imager with a deformable mirror to correct wavefront aberrations of the subject's eye. The second component was a Shack-Hartman wavefront sensor system that controlled the deformable mirror. These two subsystems were designed and optimized in house. The third subsystem was a low-resolution, wide-field imaging system,[21] with a 30° of field of view, so that the correct sampling of fundus locations could be obtained rapidly and in succession. Both AOSLO systems used a deformable mirror with a moderate stroke capable of correcting most of the wavefront aberrations of the eye (Boston Micromachines, Cambridge, MA). The second system[21,23,24] also incorporated a second deformable mirror (Imagine Eyes, Orsay, France) in a woofer–tweeter configuration. For retinal imaging, both systems used low-coherence light sources to reduce noise due to speckle. The first system used the output of an 840-nm superluminescent diode (Superlum, Moscow, Russia), the second system used the output of a supercontinuum light source (Fianium, Beverly, MA), sent through a filter with an 840-nm center wavelength and 12-nm bandwidth (Semrock, Rochester, NY). Each retinal image was 1.8° × 1.6° visual angle and the digital sampling was approximately 1 μm/pixel. For wavefront sensing, the first system used a 680 nm SLD, and the second system used light from the supercontinuum source filtered to 740 nm. Both systems used a 12-bit 1024 × 1024 CCD (Uniq Vision, Santa Clara, CA) as the detector for wavefront sensing in combination with lenslets with a 300 μm aperture and 7 mm focal length. All data were collected using a 100 μm confocal aperture (approximately two times the size of the Airy disc).

Procedures

Imaging. Wide-field fundus images were acquired in a pre-session, using en face, near-IR SLO imaging and spectral domain OCT system (Spectralis, Heidelberg Engineering GmbH, Heidelberg, Germany). The wide-field SLO images were referenced during AOSLO imaging to help locate the imaging region. For the second session, subjects' pupils were dilated with 0.5% tropicamide, with a dilated pupil size of at least 6 mm required for inclusion in the study. A three-axis chin rest and forehead pad system was used to align the subject's pupil to the imaging systems' pupil. During AO imaging, the live, wide-field image of the eye allowed direct visualization of the retinal region being imaged and comparison to the planned sampling pattern.

Because an adaptive optics system can only optically correct a small region of retina[16,25] at a time (~2° × 2°), we had to obtain many small-field image sequences arranged in a strip pattern of approximately 12° × 1.8° and including the fovea. For each small-field region we obtained approximately 1.8° × 1.6° images at 30 Hz. We sampled 50 to 100 images at one location and then repositioned the field by approximately 1°, providing the next sequence with 0.5° or more of overlap. This process was continued for the entire meridian, ensuring that the subject's pupil remained aligned with the instrument's pupil. Each strip started from the fovea and proceeded toward the peripheral retina along the four primary meridians (superior, inferior, nasal, and temporal). The result was four orthogonal strips of cone photoreceptor images recorded as an .avi file saved on disc, one for each of the four meridians. The whole procedure for AOSLO imaging on each subject took approximately 30 to 50 minutes.

Image Averaging and Montage Formation. Off-line, we assembled groups of images to generate a large montage. To create cone photoreceptor images of a given region of the retina, we typically averaged 15 to 30 video frames after the imaging session. Individual frames for averaging were selected by the operator who used a file browser (written in MatLab, The MathWorks, Natick, MA). For each local region, a frame with good image quality and minimal eye-movement–induced spatial distortions was chosen by the experimenter as a template frame, and then successive frames were aligned with the template frame. To perform precise image alignment, the retinal images were separated into small horizontal strips approximately 100 μm wide and 15 μm high. The cross-correlation of the strips and a slightly larger strip from the template was calculated, and then the maximum of the cross-correlation was used to compute the displacement of each image for each strip. These displacements, expressed as displacement as a function of time, were interpolated for every pixel in the image. The pixels were then displaced to align with the template image, in a manner similar to the approach of Stevenson and Roorda.[26] After the averaged image of a small field of the retina was created, image montaging was performed offline manually by finding overlapping points between the selected averaged images using image-analysis software (Photoshop CS3; Adobe Systems, San Jose, CA). To relate the averaged images to each other, skew and rotation were sometimes needed to align individual images. All montages were verified by comparison to the subject's wide-field SLO images (Heidelberg Engineering, Heidelberg Germany). Figure 1 shows a montage of the fovea and inferior retina from subject 5 and a wide-field SLO image of the eye in comparison.
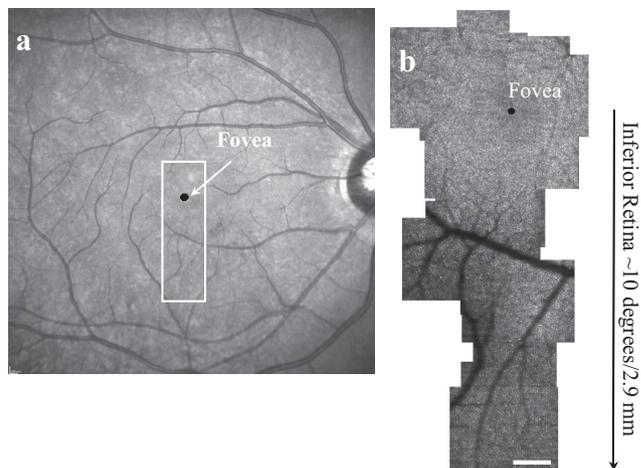

FIGURE 1. (a) Wide-field fundus image of subject 5. High-resolution AOSLO images were acquired in the boxed region. (b) High-resolution AOSLO image of fovea and inferior retina, acquired within the boxed region in (a). Scale bar, 200 μm.

Foveal Montage Generation and Determination of the Foveal Center. During AOSLO imaging, subjects were asked to look at the center of the scan raster and then at each corner. A full montage of cone photoreceptor images around the foveal center was generated from these images. The foveal center reference point for retinal coordinates was then determined by finding the center of the raster image when the subjects fixated on the center compared with the overlapping area of the four images when the subjects fixated on the four corners of the scan raster. While this technique has some errors arising from both uncertainty in bias and eye movements[27] within the frame sequence, we expect these to be within 50 μm and for distances greater than 0.3 mm, the proportional error in our retinal locations are relatively small, and no systematic bias for cone packing densities on superior, inferior, nasal, and temporal meridians was found, suggesting that our coordinates were approximately centered on the fovea.

Determination of Cone Photoreceptor Locations and Cone Density Computation. Montages for all four retinal meridians (superior, inferior, nasal, and temporal) and fovea were generated. As fiducial marks for comparison along the four meridians, 30 to 40 concentric circles centered at the fovea were plotted with 90-μm intervals between each circle. The distance of each circle was calculated from the Indiana model eye,[28] with appropriate adjustments for axial length variations. A 50 $\times$ 50-μm window of the AOSLO montage was selected along each meridian from 0.18 to 3.5 mm at every 90-μm eccentricity referenced by these concentric circles. All cone packing densities and eccentricities were thereby corrected based on the axial length of the individual subject, according to the Indiana model eye.[6,28] When vessels or defects in the image quality were noted along the meridian, the sampling regions were slightly displaced along the concentric circle to obtain the sample. With these slight adjustments, typically all the cones within a region of interest can be counted, with the exception of some cones underneath retinal blood vessels. A custom program (MatLab; The MathWorks) was used to locate cone photoreceptor positions semiautomatically[5] from each of the 50 $\times$ 50-μm windows. Manual editing was performed by the investigator to correct the cone photoreceptor positions located by the program. For every location on the four meridians, eccentricity was computed as the distance between the center of each window and the foveal center.

Missing Cone Packing Density Interpolation. While cone photoreceptors were optically resolved for most retinal locations in all the subjects, occasionally a region was missing, either due to poor image quality or an overlying blood vessel. If a statistical analysis required a sample in a region that was missing, we used exponential fitting to calculate the curve of the cone packing density as a function of retinal location (Fig. 2) and then interpolated the missing cone packing density at the specific retinal location. The filled circles in Figure 2 show the actual cone density for measured locations, and the $\times$ shows the interpolated value. This interpolation was required for only a few locations and in only three of the subjects. For the
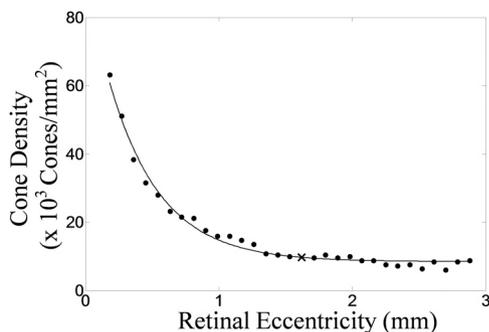
interpolations, there were always nearby points that constrained the curve fit.

Comparing Images and Cone Packing Density from Two Systems and Repeatability. Although the two AOSLO systems were configured to produce identical sampling, we further verified the calibrations by making measurements of the right eye of one of the subjects with both systems. Full montages of cone photoreceptors on the four retinal meridians were generated from the same subject, and individual cone photoreceptors were located as described above. The density estimates for a single subject, obtained from montages generated by the different systems were within 3%. To compare the cone photoreceptor distribution over time, the same retinal location (1 mm on the nasal retina) from the same subject was imaged at two times separated by 6 months, using the same AOSLO system, with the results described below.

Statistical Analysis. We performed a three-way ANOVA for the statistical analysis of cone packing density (SPSS 17; IBM, Armonk, NY). We regarded $P < 0.05$ as a statistically significant difference. When multiple tests were performed, a Bonferroni correction was applied to the significance level. To test the significance of the difference between the average results of groups 1 and 2, we computed the averaged cone packing densities for all subjects at 0.18, 0.27, 0.36, 0.45, 0.54, 0.72, 0.9, 1.08, 1.35, 1.62, 1.89, and 2.16 mm, as presented in Table 1. We chose an uneven step size because the rate of change in cone packing density with eccentricity is larger near the fovea than farther away. The coefficient of variation for the younger group was used to analyze the variation of cone density at different retinal eccentricities.

Results

Cone Packing Density in the Same Subject at Different Times

No difference in cone photoreceptor distribution was found in the same subject over the 6-month interval. Individual cone photoreceptors were found at the same location in these two images. Separate counting for the two data sets produced density estimates within 2% (Fig. 3). However, as has been reported, there are some changes in the brightness of individual cones.[29-31]

Individual Variations in Cone Packing Density

Marked individual differences in cone packing density were measured within each age group. Figure 4 shows small regions of the measured montages for all subjects. The images in the top two rows are from group 1 (younger subjects) and the bottom two rows are from group 2 (older subjects). All the images are from a location 0.81 mm ($\sim$2.8°) from the fovea in the nasal retina. The image size is 200 $\times$ 200 μm, corrected for axial length differences, which is at most 15%. Similar to other locations, cone packing density at this location varied, in this case by $\sim$50% for subjects within each age group, from 16.1 $\times$ 10^3 to 25.6 $\times$ 10^3 cones/mm^2 (younger group) and from 15.9 $\times$ 10^3 to 22.4 $\times$ 10^3 cones/mm^2 (older group).

Cone Packing Density Variation with Eccentricity and Meridian

Cone packing density varied as expected with changes in retinal eccentricity, systematically decreasing from the fovea toward the periphery in all subjects along all meridians. Because of pupil size and sampling limitations, we did not regularly sample the central foveal cone photoreceptors. We did sample from approximately 0.3° to 12° in most of the subjects. Figure 5 shows a cone photoreceptor image montage from the temporal meridian of subject 3 (axial length, 23.8 mm), demonstrating the change from 0° to a retinal eccentricity of 10°.

FIGURE 2. Exponential fitting of cone packing density at the nasal retina from subject 5. Cone packing density ($\times$10^3 cones/mm^2) is plotted as a function of retinal eccentricity (mm). (●) The actual cone densities at different retinal locations; $\times$ the interpolated cone density at 1.6-mm eccentricity.

TABLE 1. Mean Cone Photoreceptor Packing Densities

	Retinal Eccentricity					
	0.18 mm	**0.27 mm**	**0.36 mm**	**0.45 mm**	**0.54 mm**	**0.72 mm**
Superior						
Group1	63.5 ± 2.3	52.7 ± 1.9	42.4 ± 2.0	34.0 ± 2.1	29.6 ± 1.9	22.1 ± 1.4
Group2	50.2 ± 2.1	46.5 ± 2.4	39.9 ± 3.1	33.7 ± 1.9	29.4 ± 1.7	23.2 ± 1.6
Inferior						
Group1	62.8 ± 4.5	55.3 ± 1.4	44.6 ± 3.3	36.3 ± 2.8	31.4 ± 2.7	23.9 ± 2.1
Group2	50.1 ± 1.7	43.6 ± 2.2	39.5 ± 1.5	31.2 ± 1.6	28.8 ± 1.7	22.8 ± 1.6
Nasal						
Group1	68.2 ± 5.4	59.7 ± 2.8	50.0 ± 2.9	43.7 ± 2.7	37.8 ± 2.2	29.1 ± 1.8
Group2	52.6 ± 4.4	48.3 ± 2.7	43.0 ± 1.8	35.6 ± 2.3	33.1 ± 2.4	27.5 ± 1.5
Temporal						
Group1	75.2 ± 7.5	59.2 ± 4.0	50.5 ± 2.4	41.2 ± 2.0	37.3 ± 1.7	28.1 ± 1.3
Group2	46.6 ± 1.9	40.7 ± 1.6	39.0 ± 3.0	35.6 ± 2.8	33.6 ± 2.4	25.8 ± 1.9

	Retinal Eccentricity					
	0.90 mm	**1.08 mm**	**1.35 mm**	**1.62 mm**	**1.89 mm**	**2.16 mm**
Superior						
Group1	18.5 ± 1.2	15.7 ± 0.8	13.1 ± 0.8	11.7 ± 0.9	10.0 ± 0.8	8.7 ± 0.5
Group2	19.0 ± 0.9	16.4 ± 1.4	12.8 ± 0.8	11.1 ± 0.7	10.0 ± 0.6	9.1 ± 0.8
Inferior						
Group1	19.4 ± 1.6	16.6 ± 1.7	12.8 ± 1.1	11.5 ± 0.9	10.2 ± 0.8	8.1 ± 0.7
Group2	18.4 ± 1.2	15.2 ± 0.8	11.3 ± 0.7	11.1 ± 0.8	8.8 ± 0.6	8.3 ± 0.7
Nasal						
Group1	24.2 ± 1.2	19.1 ± 1.5	16.8 ± 1.5	14.5 ± 1.4	11.9 ± 0.9	10.4 ± 0.6
Group2	22.5 ± 1.1	20.9 ± 1.2	17.6 ± 1.3	15.4 ± 1.4	12.4 ± 0.8	13.0 ± 1.2
Temporal						
Group1	24.1 ± 1.5	19.9 ± 1.4	16.3 ± 0.9	13.2 ± 1.0	11.5 ± 0.5	9.7 ± 0.7
Group2	22.0 ± 1.5	18.3 ± 1.2	14.9 ± 0.8	13.3 ± 0.6	11.0 ± 0.7	9.0 ± 0.9

Data are expressed as $\times 10^3$ cones/mm^2 with standard error obtained from two groups at different retinal eccentricities at four meridians of the retina; group 1 (22–35 y), group 2 (50–65 y).

Expanded regions of the montage are presented below the montage. The eccentricities for images 1 through 4 are 1°, 4°, 7°, and 10°, respectively.

The measured cone packing densities for all four meridians are shown in Figure 6. Cone packing density was highest close to the fovea and decreased along the four meridians. Curves obtained from Curcio et al.[2] are depicted as a solid line. At 90-μm eccentricity, the cone density reached as high as 120 × 10^3 cones/mm^2. The cone packing density dropped to ~14.4 × 10^3 to 30.4 × 10^3 cones/mm^2 at 0.9-mm eccentricity and then dropped to ~7 × 10^3 cones/ mm^2 at 3.5-mm retinal eccentricity. We also found a consistent variation in packing density with meridian, with isodensity contours oriented horizontally[2,5] producing a "cone streak" ($P < 0.05$, Table 2).
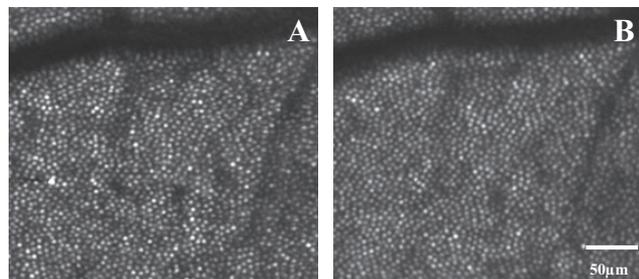

FIGURE 3. Cone distribution measured 6 months apart at the same retinal location, 1 mm eccentricity in nasal retina of subject 7. **(A)** Earlier image; **(B)** later image. Separate counting for the two images produced density estimates within 2%.

Cone Packing Density Variation with Age

There were systematic differences in cone packing density between the two age groups. The differences between groups occurred for eccentricities 1 mm or less from the fovea. In both age groups, cone packing density was high near the fovea and dropped rapidly with increasing retinal eccentricity. However, the perifoveal density (within 0.45-mm radius) was lower in the older group than in the younger group ($P < 0.0042$, Table 3).

Table 1 shows the average cone packing density with SE of each subject from the two age groups. The three-way ANOVA indicated significant differences for main effects of age, meridian, and retinal eccentricity ($P < 0.0001$) with significant interaction between age and eccentricity, age, and meridian ($P < 0.0001$, Table 4).

To test at what eccentricity there is a significant difference of cone packing density between the two age groups, post hoc analysis was performed using multiple tests and Bonferroni correction of the significance level to $P < 0.0042$. This analysis showed that the significant differences occur for the retinal locations within the central 0.45 mm (radius) of the retina. Table 3 shows the comparisons (P and effect size) tested at different retinal eccentricities, using the data of all eccentricities.

Figure 7 plots the averaged cone packing density from retinal eccentricity at 0.18, 0.27, 0.36, 0.45, 0.54, 0.72, 0.9, 1.08, 1.35, 1.62, 1.89, and 2.16 mm of the two groups. Figure 7A shows the vertical meridian (superior and inferior) of retina, and Figure 7B shows the horizontal (nasal and temporal) me-
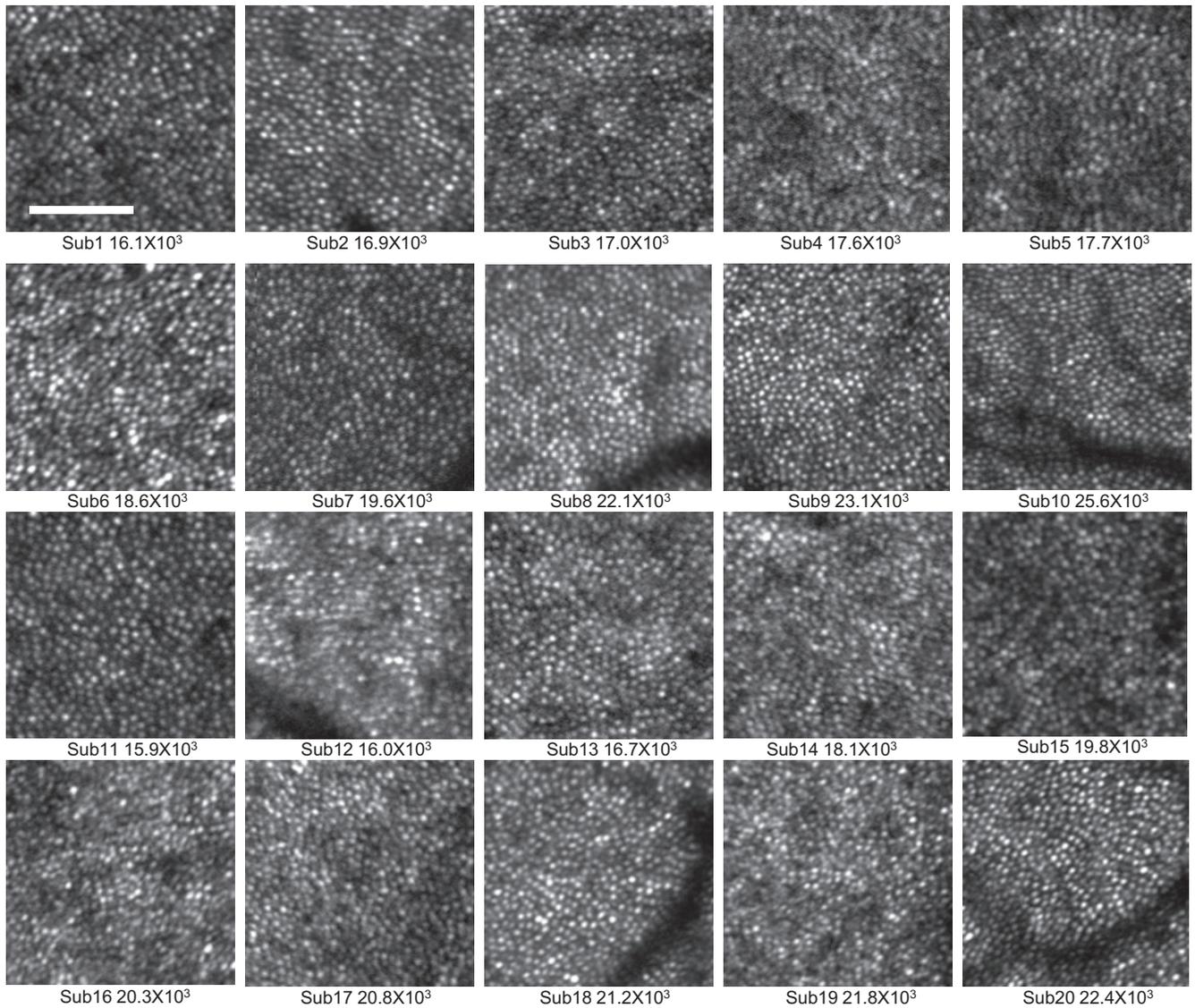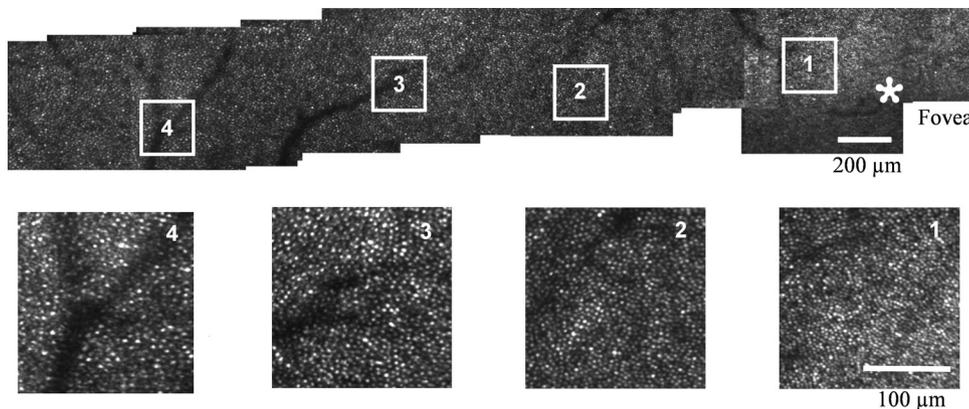
FIGURE 4. Cone photoreceptor images from a 0.81-mm eccentricity of the nasal retina for all 20 subjects. Individual images are 200×200 μm. Numbers below each panel are the cone packing density of each subject at this location in cones per square millimeter. *Top two rows*: group 1 (22–35 years); *bottom two rows*: group 2 (50–65 years). Scale bar, 100 μm.

ridian of the retina. Error bars are the SE of cone packing density.

To test the cone packing density decrease along different meridians from fovea to peripheral retina, we performed a post hoc test. No significant differences were measured between superior and inferior or nasal and temporal meridian, but there were significant differences between the orthogonal meridians ($P < 0.0001$, Table 2).

FIGURE 5. *Top*: montage of cone photoreceptors from the fovea to approximately 12° for subject 3 (axial length 23.85 mm). *Bottom*: cone photoreceptor images of subregions of the montage indicated by the squares in the *top row* montage with the corresponding numbers. Scale bar: top, 200 μm; bottom, 100 μm.
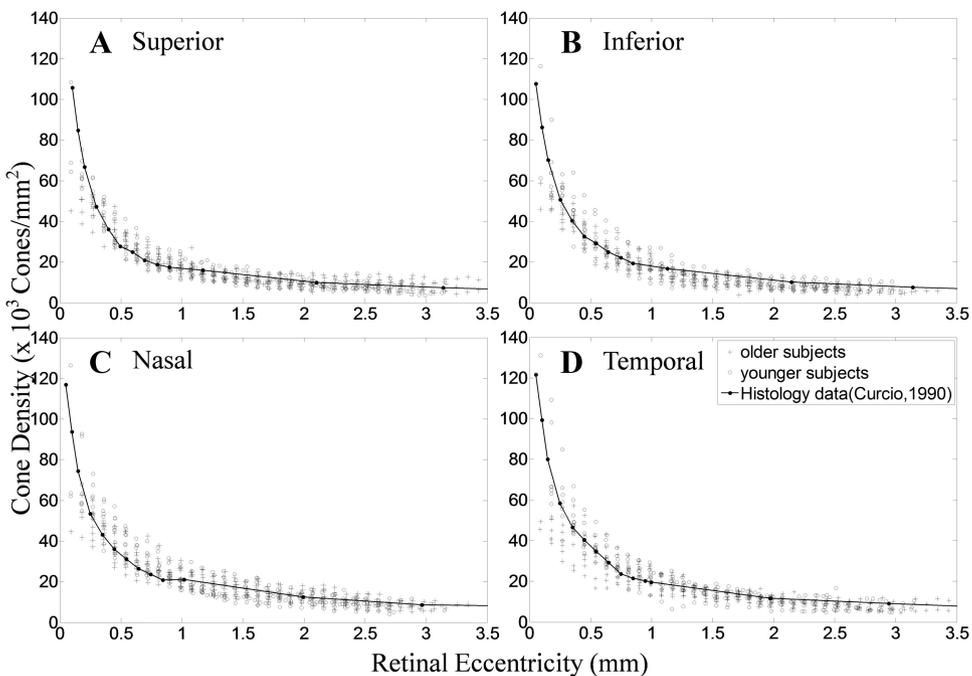
Figure 6. Cone packing density at different retinal eccentricity along four meridians from both groups. The cone density from (**A**) superior, (**B**) inferior, (**C**) nasal, and (**D**) temporal retina is shown. Group 1 was aged 22 to 35 years, group 2, 50 to 65 years. Cone densities replotted Curcio et al.[2] are shown.

Discussion

Aging and Cone Photoreceptor Packing Density

There is disagreement in the literature concerning the effects of age on cone packing density. Curcio et al.[14] found a non-significant change in the number of cone photoreceptors with age. However, they reported that the range of peak density variation at older ages was narrower, overlapping the lower end of the cone density from younger subjects. In our study, the cone density variation was narrower in the older group and overlapped the lower end of the cone density from the younger group when close to the fovea, which is consistent with the results of Curcio et al. Pandajonas et al.[12] reported an 18% decrease of cones in a lifespan of 100 years. They proposed that this discrepancy with the results of Curcio et al. arose due to the smaller number of eyes in Curcio et al., and especially to the variation in the age distribution of the sample. It is also important to note that Curcio et al. averaged the number of cones within the region of 0.8 mm around the fovea, which strongly weights the average toward the peripheral portions of that sample region, simply on an areal basis. While cone density in the center of the fovea can reach 200 $\times$ 10^3 cones/mm^2, the density decreases rapidly with increasing retinal eccentricity, and the total number of cones is still weighted toward the outer edges of their sample. Our approach emphasizes the local density of the cones rather than the areal total. Thus, we found that a significant decrease in

cone photoreceptor packing density occurred primarily at distances less than 0.5 mm from the center of the fovea. Thus, at 0.18, 0.27, 0.36, and 0.45 mm, we found that the averaged cone packing density in the older group was roughly 75%, 80%, 85%, and 90% of the average cone density in the younger group, respectively. Yet at 0.9 mm, no difference was found between the two age groups.

Our results cannot be explained by the lower densities in older subjects arising from imaging artifacts or biases, for instance due to smaller pupil sizes with age and therefore a lower resolution. As an example, Figure 8 shows cone photoreceptor images at 0.27 and 0.9 mm eccentricity on the superior retina from one older subject who showed a marked flattening of the density profile (top row) and one typical young subject (bottom row). All the cones are readily resolved in the older subject, and it is clear that the number of cones did not change proportionally with position, as it did in the younger subject.

As mentioned above, there are mixed results of human histology on age-related changes in cone packing. It is clear that nonhuman primates undergo changes in the central retina

Table 2. Comparisons of Different Meridians of Retinal Cone Packing

Pairwise Comparisons		*P*
Inferior Retina	Nasal Retina	<0.0001
	Superior Retina	1
	Temporal Retina	<0.0001
Nasal Retina	Temporal Retina	0.287
	Superior Retina	<0.0001
Superior Retina	Temporal Retina	<0.0001

P < 0.05 is regarded as statistically significant.

Table 3. Comparison of Cone Packing Density from Two Age Groups for Every Retinal Eccentricity

Different Retinal Eccentricity (mm)	*P*	Cohen's d
0.18	<0.0001	1.652758
0.27	<0.0001	1.593228
0.36	<0.0001	0.866612
0.45	0.004	0.681213
0.54	0.078	0.404635
0.72	0.461	0.165768
0.90	0.276	0.245521
1.08	0.894	0.029756
1.35	0.479	0.159003
1.62	0.966	−0.00952
1.89	0.458	0.167955
2.16	0.372	−0.20444

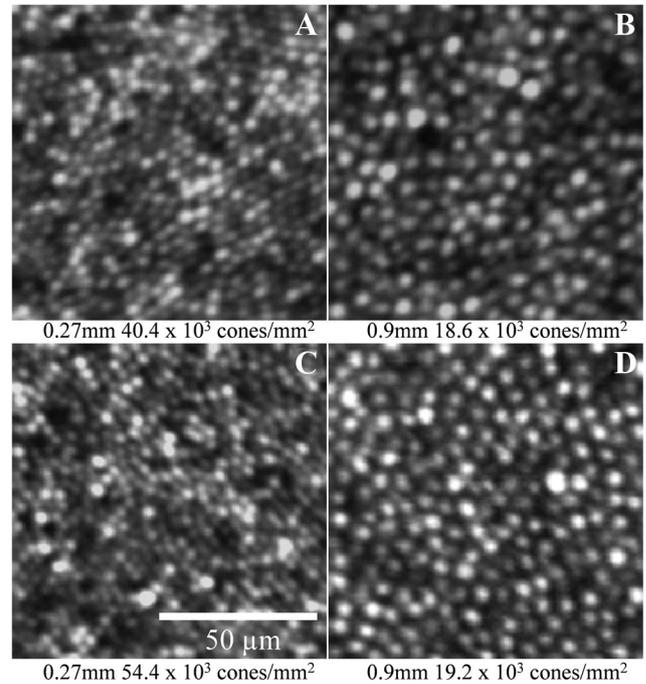*P* < 0.0042 was regarded as statistically significant.

TABLE 4. Comparison of Main Effect and Interaction Effect of Age Group, Meridian and Retinal Eccentricity of Cone Packing Density

Comparison of 3-way ANOVA	P
Main Effect of age group	<0.0001
Main effect of meridian	<0.0001
Main effect of retinal eccentricity	<0.0001
Age group × meridian	<0.0001
Age group × retinal eccentricity	<0.0001
Meridian × retinal eccentricity	0.996
Age group × meridian × retinal eccentricity	0.542

with age.[32,33] Ordy et al.[34] studied the visual acuity and foveal cone density in the retina of aged rhesus monkeys, finding that the foveal cone photoreceptor density decreased significantly in the oldest age group of macaque monkeys compared with the middle age group. Other properties of the cone photoreceptors have been found to change with age, in addition to the cone packing density. Although the photopigment density for larger fields (4°) was not found to change with age by Elsner et al.,[35] at the center of the fovea there was reduced fovea cone photopigment that matched the pattern of reduced macular pigment in older people.[4,11] Gartner and Henkind[36] reported loss of photoreceptor nuclei. Keunen et al.[9] and Kilbride et al.[37] found that the cone pigment density decreased as a function of age. Elsner et al.[11] showed that young healthy people typically have steep foveal peaks in photopigment density, but older people have shallower distributions. Our result shows that the cone packing density decreased with aging within 1 mm of the central retina, but we did not address these changes in photopigment within the cones. It is possible that both cone density and photopigment effects are linked.

Changes in the central fovea are also evident from the analysis of foveal shape by Gorrand and Delori,[38] who found that the curvature of the foveola increases with increasing age. Elsner et al.,[11] Bone et al.,[39] and Chang et al.[40] found changes in the distribution of macular pigment with age, but Delori[41] did not. Since macular pigment is deposited preferentially in the photoreceptor axons and inner plexiform layers of the retina, our finding of lower cone photoreceptor density in the older subjects is consistent with a decrease in macular pigment. Similarly a loss of cones could cause an increased curvature. An alternative possibility is that central cones spread outward, and the foveal curvature increases due to this spread, but again, the mechanism would be more complex and not easily tested by cone packing measurements alone.

As the first stage of vision, the cone photoreceptors provide spatial information to later stages of visual processing. Thus, our finding of a decrease in cone packing density within the central 0.9 mm of the fovea suggests that at least some of the decrement in decreased visual function with age is related to cone loss, although exact predictions[42,43] of acuity for a pho-

0.27mm 40.4 x 10³ cones/mm²   0.9mm 18.6 x 10³ cones/mm²

50 µm

0.27mm 54.4 x 10³ cones/mm²   0.9mm 19.2 x 10³ cones/mm²

FIGURE 8. Cone photoreceptor images from one older subject and one young subject from the superior retina. (**A**) Older subject, 0.27 mm; (**B**) older subject, 0.9 mm; (**C**) younger subject 0.27 mm; and (**D**) younger subject 0.9 mm.

toreceptor array with even small amounts of disorder are not easy. Nevertheless, such a loss can be expected to produce visual changes in the absence of other compensatory factors.

Cone Packing Density Variation between Subjects

As in previous studies, we find marked individual differences in cone packing density within both age groups.[1,3,6] In our previous study, we described individual differences in cone packing density that were related to axial length.[6] Here, we have excluded myopia greater than 4 D, and axial lengths were all between 22.1 and 26.3 mm, yet the large individual differences remained, even after correction for the axial length. According to Curcio et al.,[2] the variation of cone packing density is highest at the foveal center and much lower when it is farther away. The difference of variation in cone packing density at different retinal eccentricities has been thought to be explained by the hypothesis that the cone packing density is related to the rate, timing, and extent of cone migration during the development of the eye.[44] However, we found considerable variability in cone packing density at all retinal eccentricities measured in our study. On a proportional basis, the coef-
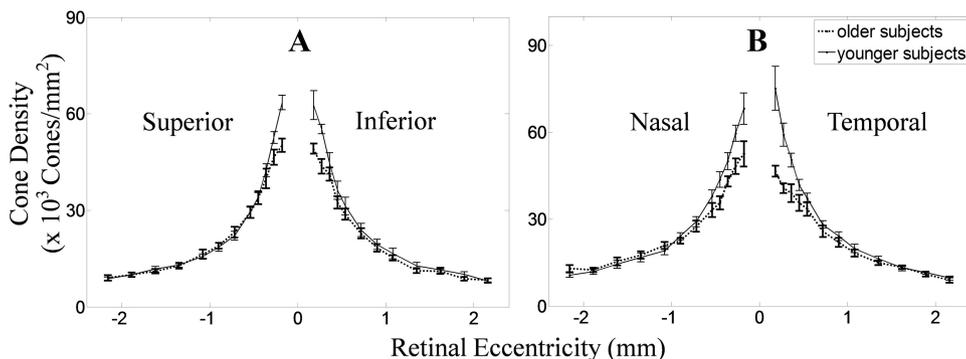
FIGURE 7. Mean cone densities from two groups as a function of eccentricity, with 0 as the center of fovea and ±1 SE shown as an error bar. (**A**) The vertical meridian retina. (**B**) The horizontal meridian retina. Shown are the average cone density in subjects from group 1 (22–35 years) and group 2 (50–65 years).

ficient of variation for the younger group at superior 0.18 mm is 22.5% and for 2.16 mm is 18.5%, which is 82% of the value closer to the fovea. An *F*-test was used to determine the significance of this observed variation of cone density at different retinal eccentricities, but the difference, while in the direction previously reported was not statistically significant in our study. Although the power to reject the null hypothesis of equal variance was low, it may have been due to a relatively small sample and large individual differences at all retinal locations. We also found that, in general, subjects with higher cone packing density at the midperipheral retina also had higher density close to the fovea, again suggesting that some of these individual variations were general and not related solely to foveal migration during development.

Computing the Retinal Magnification Factor

Currently, different model eyes are used to compute retinal magnification factor (RMF), including the method developed by Bennett et al.,[45] the Gullstrand model eye,[46] and the Indiana model eye,[47] among others. Although the RMFs calculated using different model eye are slightly different, the difference is small. For example, for eyes with axial length within 22 to 26.5 mm, the differences in RMF calculated using any of the methods listed above are less than 2%. No direct evidence shows which model eye is the most accurate one. In our study, we used the Indiana model eye to compute RMF for different subjects. Another consideration in scaling the cone packing densities is that the axial length of the eye is not identical across the retina. In our study, we imaged the retinal from 0.6° to 12°. We do not expect that this had a major impact on our conclusions since the axial length measured at 0.6° is only approximately 0.4% different from the axial length measured at 12°,[48] on average. Thus, we used a single value of axial length to calculate the RMF from 0.6° to 12°.

Limitation of AOSLO Imaging in Two Different Age Groups

Cone photoreceptors in subjects of different ages were imaged in our study. Because resolution depends on pupil size and contrast, we are not always able to measure cones at the center of the fovea, although in most subjects, we map cones that are quite close. In general, image quality was better in the young subjects than in older subjects. This limitation could arise from several factors: (1) Changes to the tear film, lens, and vitreous with increasing age can increase scattering and possibly increases in very high order aberrations that are not fully corrected by our AOSLO system; (2) as mentioned, pupils in the older subjects, even when dilated with pharmacologic agents tended to be smaller[49]; and (3) in at least some of the older subjects, there seemed to be marked increases in inner retinal scattering. This effect was seen as a fairly high-contrast image of the inner retina and nerve fiber layer, but decreased image quality for the photoreceptor images. In all subjects used for this analysis, high-quality cone photoreceptor images were obtained beyond 1° from the foveal center. For many subjects, there are quantifiable cone data within the central 180 μm of the fovea, although we did not include these in the statistical analysis, since there were too many missing data points.

CONCLUSION

We found a decrease in cone photoreceptor packing density of up to 25% in older as opposed to younger subjects. This decrease was found primarily within 0.45 mm of the foveal center, and beyond that eccentricity, older subjects did not differ from the younger subjects. Our results are consistent with other studies suggesting changes in foveal architecture with age.

References

1. Curcio CA, Sloan KR Jr, Packer O, Hendrickson AE, Kalina RE. Distribution of cones in human and monkey retina: individual variability and radial asymmetry. *Science.* 1987;236:579–582.
2. Curcio CA, Sloan KR, Kalina RE, Hendrickson AE. Human photoreceptor topography. *J Comp Neurol.* 1990;292:497–523.
3. Curcio CA, Sloan KR. Packing geometry of human cone photoreceptors: variation with eccentricity and evidence for local anisotropy. *Vis Neurosci.* 1992;9:169–180.
4. Elsner AE, Berk L, Burns SA, Rosenberg PA. Aging and human cone photopigments. *J Opt Soc Am A.* 1988;5:2106–2112.
5. Chui TY, Song H, Burns SA. Adaptive-optics imaging of human cone photoreceptor distribution. *J Opt Soc Am A.* 2008;25:3021–3029.
6. Chui TYP, Song H, Burns SA. Individual variations in human cone photoreceptor packing density: variations with refractive error. *Invest Ophthalmol Vis Sci.* 2008;49:4679–4687.
7. Marshall J, Grindle J, Ansell PL, Borwein B. Convolution in human rods: an ageing process. *Br J Ophthalmol.* 1979;63:181–187.
8. Marshall J. Ageing changes in human cones. In: Shimizu K, Oosterhuis JA, eds XXIII Concilium Ophthalmologicum, Kyoto, Japan. Amsterdam: Elsevier North-Holland; 1978;375–378.
9. Keunen JEE, Norren Dv, Meel GJv. Density of foveal cone pigments at older age. *Invest Ophthalmol Vis Sci.* 1987;28:985–991.
10. Swanson WH, Fish GE. Age-related changes in the color-match-area effect. *Vision Res.* 1996;36:2079–2085.
11. Elsner AE, Burns SA, Beausencourt E, Weiter JJ. Foveal cone photopigment distribution: small alterations associated with macular pigment distribution. *Invest Ophthalmol Vis Sci.* 1998;39:2394–2404.
12. Pandajonas S, Jonas JB, Jakobczykzmija M. Retinal photoreceptor density decreases with age. *Ophthalmology.* 1995;102:1853–1859.
13. Gao H, Hollyfield JG. Aging of the human retina differential loss of neurons and retinal-pigment epithelial-cells. *Invest Ophthalmol Vis Sci.* 1992;33:1–17.
14. Curcio CA, Millican CL, Allen KA, Kalina RE. Aging of the human photoreceptor mosaic: evidence for selective vulnerability of rods in central retina. *Invest Ophthalmol Vis Sci.* 1993;34:3278–3296.
15. Roorda A, Romero-Borja F, Donnelly W III, Queener H, Hebert T, Campbell M. Adaptive optics scanning laser ophthalmoscopy. *Opt Express.* 2002;10:405–412.
16. Liang J, Williams DR, Miller DT. Supernormal vision and high-resolution retinal imaging through adaptive optics. *J Opt Soc Am A.* 1997;14:2884–2892.
17. Song H, Zhao Y, Qi X, Chui YT, Burns SA. Stokes vector analysis of adaptive optics images of the retina. *Opt Lett.* 2008;33:137–140.
18. Zhong ZY, Petrig BL, Qi XF, Burns SA. In vivo measurement of erythrocyte velocity and retinal blood flow using adaptive optics scanning laser ophthalmoscopy. *Opt Express.* 2008;16:12746–12756.
19. Roorda A, Zhang YH, Duncan JL. High-resolution in vivo imaging of the RPE mosaic in eyes with retinal disease. *Invest Ophthalmol Vis Sci.* 2007;48:2297–2303.
20. Song H, Qi X, Zou W, Zhong Z, Burns SA. Dual electro-optical modulator polarimeter based on adaptive optics scanning laser ophthalmoscope. *Opt Express.* 2010;18:21892–21904.
21. Ferguson RD, Zhong Z, Hammer DX, et al. Adaptive optics scanning laser ophthalmoscope with integrated wide-field retinal imaging and tracking. *J Opt Soc Am A.* 2010;27:A265–A277.
22. Burns SA, Tumbar R, Elsner AE, Ferguson D, Hammer DX. Large-field-of-view, modular, stabilized, adaptive-optics-based scanning laser ophthalmoscopy. *J Opt Soc Am A.* 2007;24:1313–1326.
23. Zou W, Qi X, Burns SA. Wavefront-aberration sorting and correction for a dual-deformable-mirror adaptive-optics system. *Opt Lett.* 2008;33:2602–2604.

24. Zhong Z, Song H, Chui TY, Petrig BL, Burns SA. Non-invasive measurements and analysis of blood velocity profiles in human retinal vessels. *Invest Ophthalmol Vis Sci.* 2011;52:4151–4157.

25. Bedgood P, Daaboul M, Ashman R, Smith G, Metha A. Characteristics of the human isoplanatic patch and implications for adaptive optics retinal imaging. *J Biomed Opt.* 2008;13:024008.

26. Stevenson SB, Roorda A. Correcting for miniature eye movements in high resolution scanning laser ophthalmoscopy. *Proc SPIE.* 2005;5688A:145–151.

27. Putnam NM, Hofer HJ, Doble N, Chen L, Carroll J, Williams DR. The locus of fixation and the foveal cone mosaic. *J Vision.* 2005;5:632–639.

28. Thibos LN, Ye M, Zhang X, Bradley A. The chromatic eye: a new reduced-eye model of ocular chromatic aberration in humans. *Appl Opt.* 1992;31:3594–3600.

29. Burns SA, Wu S, Delori F, Elsner AE. Direct measurement of human-cone-photoreceptor alignment. *J Opt Soc Am A.* 1995;12:2329–2338.

30. Jonnal RS, Rha J, Zhang Y, Cense B, Gao W, Miller DT. In vivo functional imaging of human cone photoreceptors. *Opt Express.* 2007;15:16141–16160.

31. Pallikaris A, Williams DR, Hofer H. The reflectance of single cones in the living human eye. *Invest Ophthalmol Vis Sci.* 2003;44:4580–4592.

32. Francis PJ, Appukuttan B, Simmons E, et al. Rhesus monkeys and humans share common susceptibility genes for age-related macular disease. *Hum Mol Genet.* 2008;17:2673–2680.

33. Ulshafer RJ, Engel HM, Dawson WW, Allen CB, Kessler MJ. Macular degeneration in a community of rhesus monkeys: ultrastructural observations. *Retina.* 1987;7:198–203.

34. Ordy JM, Brizzee KR, Hansche J. Visual-acuity and foveal cone density in the retina of the aged rhesus-monkey. *Neurobiol Aging.* 1980;1:133–140.

35. Elsner AE, Burns SA, Webb RH. Mapping cone photopigment optical density. *J Opt Soc Am A.* 1993;10:52–58.

36. Gartner S, Henkind P. Aging and degeneration of the human macula. 1. Outer nuclear layer and photoreceptors. *Br J Ophthalmol.* 1981;65:23–28.

37. Kilbride PE, Hutman LP, Fishman M, Read JS. Foveal cone pigment density difference in the aging human eye. *Vision Res.* 1986;26:321–325.

38. Gorrand JM, Delori FC. Reflectance and curvature of the inner limiting membrane at the foveola. *J Opt Soc Am A.* 1999;16:1229–1237.

39. Bone R, Landrum J, Fernandez L, Tarsis S. Analysis of the macular pigment by HPLC: retinal distribution and age study. *Invest Ophthalmol Vis Sci.* 1988;29:843–849.

40. Chang Y, Lee FL, Chen SJ, Chen SF. Optical measurement of human retinal macular pigment and its spatial distribution with age. *Med Phys.* 2002;29:2621–2628.

41. Delori FC. Autofluorescence method to measure macular pigment optical densities fluorometry and autofluorescence imaging. *Arch Biochem Biophys.* 2004;430:156–162.

42. Yellott JI. Spectral analysis of spatial sampling by photoreceptors: topological disorder prevents aliasing. *Vision Res.* 1982;22:1205–1210.

43. Yellott JI. Spectral consequences of photoreceptor sampling in the rhesus retina. *Science.* 1983;221:382–385.

44. Hendrickson AE, Yuodelis C. The morphological development of the human fovea. *Ophthalmology.* 1984;91:603–612.

45. Bennett AG, Rudnicka AR, Edgar DF. Improvements on Littmann's method of determining the size of retinal features by fundus photography. *Graefes Arch Clin Exp Ophthalmol.* 1994;232:361–367.

46. de Almeida MS, Carvalho LA. Different schematic eyes and their accuracy to the in vivo eye: a quantitative comparison study. *Braz J Phys.* 2007;37:378–387.

47. Thibos LN, Ye M, Zhang X, Bradley A. The chromatic eye: a new reduced-eye model of ocular chromatic aberration in humans. *Appl Opt.* 1992;31:3594–3600.

48. Mallen EAH, Kashyap P. Technical Note: Measurement of retinal contour and supine axial length using the Zeiss IOLMaster. *Ophthalmic Physiol Opt.* 2007;27:404–411.

49. Yang YB, Thompson K, Burns SA. Pupil location under mesopic, photopic, and pharmacologically dilated conditions. *Invest Ophthalmol Vis Sci.* 2002;43:2508–2512.